NUMERICAL MODELING OF AN ACTIVE NOISE REDUCTION SYSTEM IN THE ENGINE EXHAUST PIPE

A. Ivantsov[1], L. Klimenko[1,2], T. Lyubimova[1,2] and B. Roux[3]

[1]Institute of Continuous Media Mechanics UB RAS, Perm, Russian Federation
[2]Perm State University, Perm, Russian Federation
[3]Aix-Marseille Université, Marseille, France

Numerical simulation of an active noise reduction system in the exhaust pipe of the internal combustion engine is being reported. It is proposed to place an additional controlled sound source into the engine exhaust pipe, which is opposite in phase to the sound waves coming from the engine. A round plate that performs rotational vibrations with a given frequency and amplitude is assumed to be such a source. The ideal gas model is used to describe the state of gas. The Realizable $\kappa - \varepsilon$ turbulence model is applied to simulate the compressible gas flow. Modeling of the additional sound source created by the damper was carried out by a direct method based on changing the position of the damper at each time step. . The damper motion was realized within the framework of the sliding mesh approach, for this, a spherical mesh segment was created round the damper, which rotates during calculations. The influence of the plate size and the incoming sound wave parameters on the operation of the active noise suppression system of an internal combustion engine has been evaluated. The dependences of the amplitude of oscillations of static and total pressure at the outlet of the noise reduction system on the amplitude and radius of the oscillating damper were obtained. The simulations were conducted for various values of the exhaust pipe radius, and the effect of the size of the expansion chamber located in front of the oscillating damper was also studied. Calculations have shown that the proposed active noise suppression system is able to reduce the engine noise level by 10 dB, while increasing the plate radius leads to an increase in the efficiency of the noise suppression system. However, at the same time, the level of aerodynamic resistance that the noise suppression system provides to the gas flow also increases, which can lead to a decrease in engine power characteristics.

Key words: compressible gas flow, numerical simulation, sliding mesh, active noise reduction

1. Introduction

Power and energy facilities that emit gas-air mixtures into the environment (vehicle engines, low-speed compressor units, blowers, stationary internal combustion engines, ventilation systems, etc.) are known to create intense acoustic radiation, which is usually a source of discomfort for the population [1–3]. A particularly serious problem is low-frequency noise due to the fact that, in contrast to rapidly decaying high-frequency waves, low-frequency noise can propagate over a considerable distance without intense reduction [4].

According to the way of functioning, noise reduction systems can be classified as dissipative, reactive, combined and active [5]. The most familiar ones are dissipative mufflers (tubular or plate) containing channels lined with sound-absorbing material. They are absorption-type silencers, where sound energy is converted into heat in a layer of sound-absorbing material. The inner tube of such mufflers is made of perforated sheet material. The use of silencers of this type is limited by the high cost of sound-absorbing material, clogging, fairly rapid material aging, and so on.

Reactive silencers reflect sound due to the formation of a "wave plug", which makes it difficult to transmit acoustic vibrations [2]. Combination mufflers use the properties of both sound absorption and reflection of sound energy. An example of a combined silencer is a chamber silencer, the inner surface of the walls of which is lined with sound-absorbing material. In this case, it is necessary to take into account the possible occurrence of resonance effects in the system [6, 7].

Recently, active noise suppressors have been increasingly used, the principle of which is to generate a wave signal of the same amplitude and frequency as the unwanted sound, but opposite in phase. The active noise suppression system was proposed by P. Lueg [8]. Active compensation is based on the principles of superposition and interference. The superposition in space (on a surface) of two or more sound (vibration) waves, as a result of which at different points in space (surface) a weakening of the resulting wave is obtained.

In most works devoted to active noise suppression systems for an internal combustion engine [9–13], systems equipped with speakers that produce sound waves of opposite phase are discussed. In this paper, we consider such a system when mechanical generation of a sound wave is carried out inside the engine exhaust

pipe. In particular, the effectiveness of the active noise reduction by a round plate placed inside the engine exhaust pipe is numerically studied. The flapper performs rotational oscillations around an axis perpendicular to the pipe which are controlled by a special motor. The simulation is carried out in order to determine optimal parameters for the noise reduction system operation and to evaluate its effectiveness, as well as, the impact on engine characteristics, such as power and torque.

2. Statement of the problem

We consider a section of the exhaust pipe, assuming that it is a cylinder of circular cross section. A round flapper is placed in the center of the pipe and can perform controlled rotational oscillations around an axis perpendicular to the pipe (Fig. 1). Let us introduce a coordinate system with the axis x directed along the pipe and the axis y that is along the axis of rotation of the flapper.

Fig. 1. Scheme of the noise reduction system with the flapper swinging inside the engine exhaust pipe.

Experimental measurement of pressure fluctuations in the engine exhaust shows the presence of a wide spectrum of noise waves, therefore, the full-scale numerical analysis based on experimental data is a very difficult task. However, the spectral analysis of the measured signal makes it possible to restrict the study to the consideration of the low-frequency harmonic associated with the engine speed, because the intensity of this harmonic is much higher than the average value. We will assume that the conditions at the input to the active noise reduction system correspond to a harmonic sound wave, the frequency of which is determined by the engine speed. Thus, at the inlet to the system, the total pressure varies according to the law:

$$P_{total}(t) = \frac{1}{2}P_{max}\left[1 - \cos(\omega t + \Delta\varphi)\right] + p_a, \qquad (1)$$

where ω is the frequency of the incoming sound wave, P_{max} is the amplitude of the pressure fluctuations, p_a is the atmospheric pressure, $\Delta\varphi$ is the problem parameter characterizing the phase difference between the pressure and the plate. The case $\Delta\varphi = 0$ corresponds to synchronous plate oscillations when at maximum inlet pressure the plate reaches the maximum deflection angle (if the maximum angle is the right angle the flapper becomes perpendicular to the plane $\{x, y\}$). The equation (1) produces both the sound wave and the average gas flow that exists in a real engine. At the outlet of the pipe, we set the condition for static pressure, which is supposed to be equal to atmospheric pressure.

The flapper performs rotational oscillations around an axis perpendicular to the pipe and the angle of inclination of the plate changes in time according to the law:

$$a(t) = a_{max}\sin\left(\frac{\omega}{2}t\right), \qquad (2)$$

where a_{max} is the maximum deflection angle of the flapper from the plane $\{x, y\}$. Note that the frequency of the plate oscillation is half of the incoming sound wave frequency, since the upper and lower positions of the plate are equivalent.

Numerical modelling is performed for the parameters of the internal combustion engine O-200 (see Fig. 2). The pipe diameter is 60 mm, its length is 0.6 m. The flapper thickness is 2 mm and the diameter is 54 mm for the most calculations except the study of the flapper diameter influence. The angle of maximum damper deflection $a_{max} = 45°$, if it is not additionally specified. The flapper is located at the center of the pipe.

The calculations are carried out for parameters of air at temperature equals 500°C. In the modelling, the gas is assumed to be ideal. A series of calculations are performed with the addition expansion chamber before the oscillating flapper (Fig. 3).

Fig. 2. Aircraft O-200 Engine.
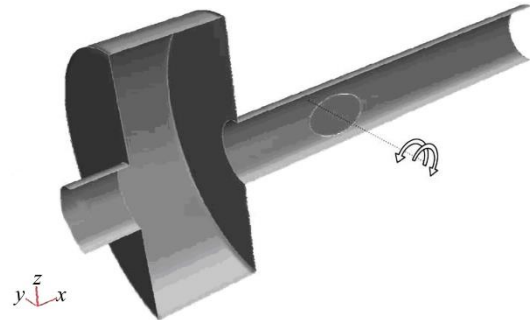
Fig. 3. Scheme of the noise reduction system with an expansion chamber.

3. Numerical method

ANSYS Fluent is used for numerical simulation of the problem. The state of the gas is described by an ideal gas model. High values of Reynolds number require the use of a turbulent gas flow model. The Realizable turbulence model was chosen for compressible gas dynamics modelling. The advantage of the Realizable model, compared to the conventional $\kappa - \varepsilon$ turbulence model, is more accurately prediction of distribution of turbulent dissipation rate for flat and round streams, and also provides better prediction of rotating flows, boundary layers subject to strong pressure gradients, separation and recirculation flows. The model removes some mathematical restrictions on the Reynolds stresses that occur in turbulent flows [14, 15]. Thus, the Realizable turbulence model has advantages over the standard model in the system under consideration due to the possible occurrence of vortex and rotating flows in it.

In accordance with the Realizable model, the evolution of turbulent kinetic energy and turbulent dissipation rate are described by the following equations [14]:

$$\frac{\partial(\rho\kappa)}{\partial t} + \frac{\partial(\rho v_j \kappa)}{\partial x_j} = \frac{\partial}{\partial x_i}\left[\left(\mu + \frac{\mu_t}{\sigma_\kappa}\right)\frac{\partial\kappa}{\partial x_i}\right] + G_\kappa + G_b - \rho\varepsilon , \tag{3}$$

$$\frac{\partial(\rho\varepsilon)}{\partial t} + \frac{\partial(\rho v_j \varepsilon)}{\partial x_j} = \frac{\partial}{\partial x_i}\left[\left(\mu + \frac{\mu_t}{\sigma_\varepsilon}\right)\frac{\partial\varepsilon}{\partial x_i}\right] + \rho C_1 S\varepsilon - \rho C_2 \frac{\varepsilon^2}{\kappa + \sqrt{\nu\varepsilon}} + C_{1\varepsilon}\frac{\varepsilon}{\kappa}G_b , \tag{4}$$

where ρ is the gas density, μ and μ_t is the gas viscosity and turbulent viscosity, G_κ is the generation of turbulent kinetic energy by inhomogeneities of the velocity field, G_b is the generation of turbulent kinetic energy, calculated by the formula,

$$G_b = \beta\mathbf{g}\frac{\mu_t}{\sigma_T}\frac{\partial T}{\partial x_i} , \tag{5}$$

where β is the gas volume expansion coefficient and σ_T is the turbulent Prandtl number. The Navier–Stokes equation and the continuity equation are

$$\frac{\partial \rho v_i}{\partial t} + \frac{\partial (\rho v_j v_i)}{\partial x_j} = \frac{\partial}{\partial x_i}\left(p + \frac{2}{3}\left(\rho \kappa + (\mu + \mu_t)\frac{\partial v_j}{\partial x_j}\right)\right) + \frac{\partial}{\partial x_j}\left((\mu + \mu_t)\left(\frac{\partial v_i}{\partial x_j} + \frac{\partial v_j}{\partial x_i}\right)\right) + \rho g_i, \qquad (6)$$

$$\frac{\partial \rho}{\partial t} + \frac{\partial (\rho v_j)}{\partial x_j} = 0 . \qquad (7)$$

The model contains the following parameters:

$$C_1 = \max\left[0,43, \frac{\eta}{\eta + 5}\right]; \qquad \eta = S\frac{\kappa}{\varepsilon}; \qquad S = \sqrt{2S_{ij}S_{ij}}; \qquad S_{ij} = \frac{1}{2}\left(\frac{\partial u_j}{\partial x_i} + \frac{\partial u_i}{\partial x_j}\right); \qquad (8)$$

$$C_{1\varepsilon} = 1,44; \qquad C_2 = 1,9; \qquad \sigma_T = 0,85; \qquad \sigma_\kappa = 1,0; \qquad \sigma_\varepsilon = 1,2 . \qquad (9)$$

Turbulent viscosity is determined by the formula:

$$\mu_t = \rho C_\mu \frac{\kappa^2}{\varepsilon}, \qquad (10)$$

where C_μ, in contrast to the constant in standard model, is the function calculated by

$$C_\mu = \frac{1}{A_0 + A_s\left(\kappa S/\varepsilon\right)} . \qquad (11)$$

Here

$$A_0 = 4,04, \qquad A_s = \sqrt{6}\cos\varphi, \qquad (12)$$

$$\varphi = \frac{1}{3}\cos^{-1}(\sqrt{6}W), \qquad W = \frac{S_{ij}S_{jk}S_{ki}}{S} . \qquad (13)$$

The accuracy of numerical simulation of turbulent flows is significantly affected by correct description of wall effect. The boundary conditions at a solid wall should take into account high viscosity dissipation at small distances from the wall that leads to formation of a thin laminar layer near the wall. Consequently, due to the large gradient of average velocity, the generation of turbulent kinetic energy takes place.

There are two usual approaches to modeling turbulent flow near a wall. The first is based on near-wall functions and the second is a low Reynolds number model.

The near-wall approach requires that the center of the cell of the first mesh point lies in the logarithmic layer. To solve the problem using the second approach, a high-resolution mesh is needed near the boundary. Both approaches lead to significant errors if used outside the range of their applicability. It is worth noting that the near-wall Re number (y^+ the parameter in the description of the logarithmic layer in the approach with near-wall functions) in the case of a complex geometry of the problem cannot be accurately calculated before solving the problem.

To avoid such disadvantages, we use the near-wall Menter–Lechner model [16] with a new approach to modeling boundary conditions. The main idea of the approach is the introduction of the source term S_{wall} to the equation of the turbulence kinetic energy transfer. Thus, the equation for turbulent kinetic energy is

$$\frac{\partial (\rho \kappa)}{\partial t} + \frac{\partial (\rho u_j \kappa)}{\partial x_j} = \frac{\partial}{\partial x_i}\left[\left(\mu_m + \frac{\mu_t}{\sigma_\kappa}\right)\frac{\partial \kappa}{\partial x_i}\right] + G_k + G_b - \rho \varepsilon + S_{wall} . \qquad (14)$$

The source term S_{wall} is necessary to correctly take into account the effects observed near the wall. It is not equal to zero only in the laminar layer near solid walls, where the characteristic Reynolds number is rather low, and it decreases down to zero in the logarithmic region with the growth of the distance from the wall.

The flapper motion is modeled using a sliding mesh model provided by Ansys Fluent. The spherical mesh segment is created around the flapper and is rotated together with the flapper during the calculations. The angular speed of the rotation is corrected at each time step in accordance with the formula (2).

The effectiveness of the noise suppression is estimated by the magnitude of the sound intensity drop in the part of the pipe under consideration. Sound intensity is a vector physical variable that characterizes the power carried by a sound wave in the direction of its propagation. It is calculated by the formulas [1–3],

$$\mathbf{I} = \left(\frac{p_a}{\rho_0} + \mathbf{v}_a \cdot \mathbf{v}_0 \right) \left(\rho_0 \mathbf{v}_a + \rho_a \mathbf{v}_0 \right), \tag{15}$$

where p_a, $\mathbf{v}_a$ and ρ_a are fluctuations in pressure, velocity and density of the gas, respectively; $\mathbf{v}_0$ and ρ_0 are time-averaged gas velocity and gas density (note that full velocity is $\mathbf{u} = \mathbf{v}_a + \mathbf{v}_0$). The projection of the gas velocity on the x axis is used for calculations of the sound intensity. The averaging is carried out over time, much longer than the period of the sound wave entering the system,

$$v_0 = \frac{1}{t_*} \int_0^{t_*} \upsilon(t)\,dt, \qquad \rho_0 = \frac{1}{t_*} \int_0^{t_*} \rho(t)\,dt.$$

Fluctuations in pressure, velocity and density of the gas are calculated by the formulas:

$$p_a(t) = p(t) - \frac{1}{t_*} \int_0^{t_*} p(t)\,dt, \tag{16}$$

$$\upsilon_a(t) = \upsilon(t) - \frac{1}{t_*} \int_0^{t_*} \upsilon(t)\,dt = \upsilon(t) - v_0, \tag{17}$$

$$\rho_a(t) = \rho(t) - \frac{1}{t_*} \int_0^{t_*} \rho(t)\,dt = \rho(t) - \rho_0. \tag{18}$$

The obtained intensity is averaged first over the pipe section, and then over the calculation time,

$$\overline{I} = \frac{1}{t_{max}} \int_0^{t_{max}} I\,dt, \tag{19}$$

where I is x projection of the sound intensity vector $\mathbf{I}$ averaged over the normal section of the pipe.

The sound intensity level in decibel is calculated by the formula [2]:

$$L = 10\log_{10}\left(\overline{I}/I_0\right), \tag{20}$$

where $I_0 = 10^{-12}$ Wt/m^2.

4. Modeling results

4.1. Influence of the external space

As mentioned above, at the outlet of the system under consideration the boundary condition for static pressure is implemented that is assumed to be constant. This simplification requires additional validation. Thus, an extra series of calculations was carried out, taking into account the gas outlet from the exhaust pipe and the presence of the external environment. The scheme of the problem and the geometry used for those calculations are shown in Figure 4.
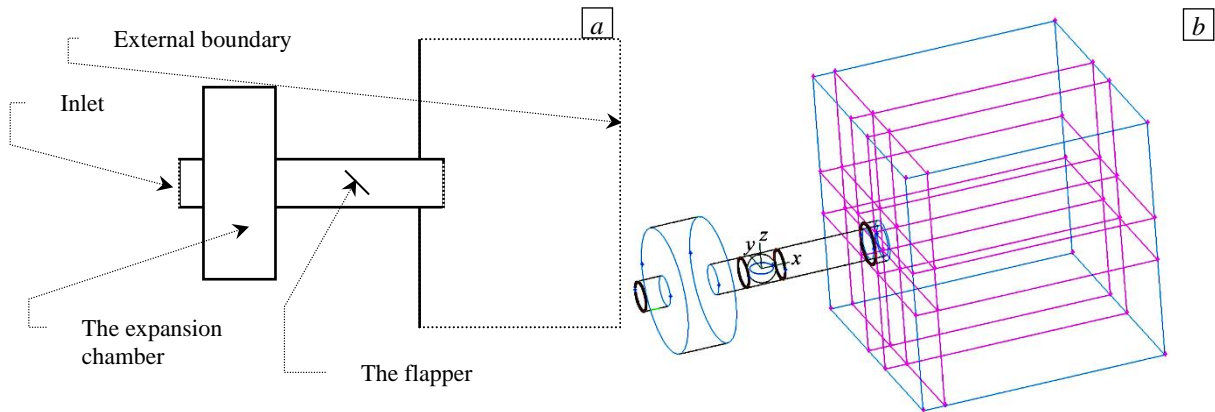
Fig. 4. Scheme (a) and geometry (b) of the problem with the external space.
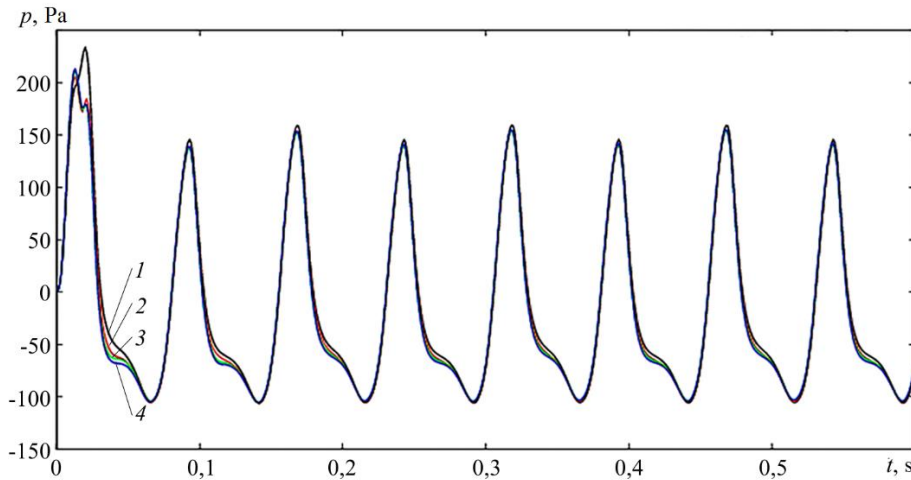
Fig. 5. Time dependence of the pressure at the outlet for different volumes of the outer area V, m^3: 0,2 (curve *1*); 0,5 (curve *2*); 1,0 (curve *3*); 1,5 (curve *4*).

4.2. Influence of the expansion chamber

This section presents the results of the study of gas flow and the noise intensity at the outlet of the exhaust pipe in the presence of an expansion chamber. As one can see in Figure 6b, the chamber presence has little effect on the flow in the pipe. At the same time, the gas flow in the additional volume of the expansion chamber is much weaker than the flow in other parts of the pipe.

The sound intensity level at the inlet and at the outlet is shown in Fig. 7 for different volumes of the expansion chamber. It can be seen from the graph that adding an expansion chamber to the system increases its efficiency, however, the dependence of the sound intensity on the volume of the expansion chamber is rather weak.

4.3. Moment of forces acting on the flapper

The ANSYS Fluent allows calculating the force acting on a solid wall from a liquid or gas flow. By integrating this force

Fig. 6. The trajectory of the movement of the exhaust gas in the pipe in the absence (a) and the presence (b) of the expansion chamber; the color of the lines corresponds to velocity magnitude.
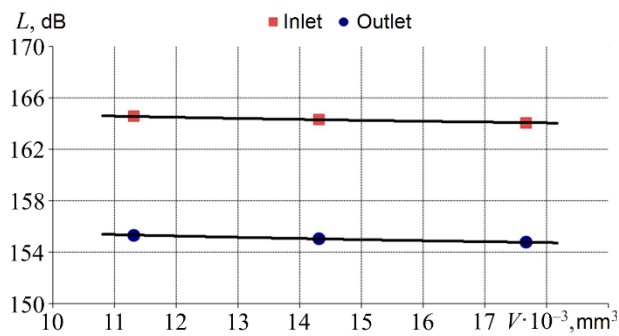
Fig. 7. Sound intensity at the inlet to and outlet of the sound suppression system for different volumes of the expansion chamber.

over the damper surface, one can obtain the moment of forces that causes its oscillations. Figure 8 shows the dependence of the moment of forces on time for various values of the flapper diameter. Since, due to the rotation of the damper, the volume of gas passing through the section of the pipe is different at different times, the moment of forces acting on the damper also changes with time.

Particularly noticeable changes occur when the damper does not interfere with the passage of the flow, that is, the pipe is completely open. The peak values of the moment are reached at the maximum deflection angle of the damper (during the complete overlap of the pipe section). It should be noted that the dependence of the moment of forces on the deflection angle of the damper is nonmonotonic. An increase in the diameter of the damper leads to an increase in the forces acting on it.
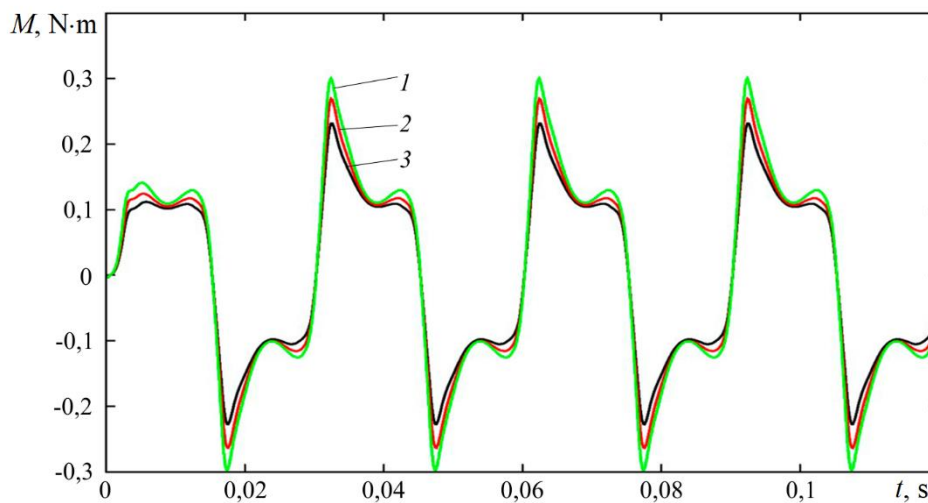
Fig. 8. Evolution of the moment of force rotating the flapper caused by gas flow for different plate diameters D: 54 mm (curve 1), 52 mm (2), 50 mm (3).

4.4. Dependence of noise reduction efficiency on system parameters

Dependences of the noise reduction efficiency are constructed for various parameters of the system under study. As a characteristic of the noise reduction efficiency, the difference between the noise levels at the outlet of the system and in its absence (in a pipe without a damper) is used.

Figure 9a shows the dependence of the noise reduction efficiency on the maximum deflection angle of the damper from the plane $\{x, y\}$. As can be seen, with an increase in the deflection angle of the damper, the noise reduction coefficient of the system increases. However, at the same time, the aerodynamic resistance that the noise reduction system exerts on the gas flow also becomes higher, which leads to a decrease in engine power.

A similar situation is observed when the damper diameter is changed (see Fig. 9b). With its increase, the noise reduction system works more efficiently, but at the same time, its aerodynamic drag increases significantly.

The result of the study of the effect on noise suppression of the phase difference between the oscillations of the damper and the sound wave at the entrance to the system is shown in Figure 9c. The greatest efficiency of the system is achieved when the damper oscillations lag behind the pressure pulsations at its inlet. Calculations have shown that the effectiveness of the noise reduction system is maximum at a phase difference $\pi/30$ (or at 6 degrees).
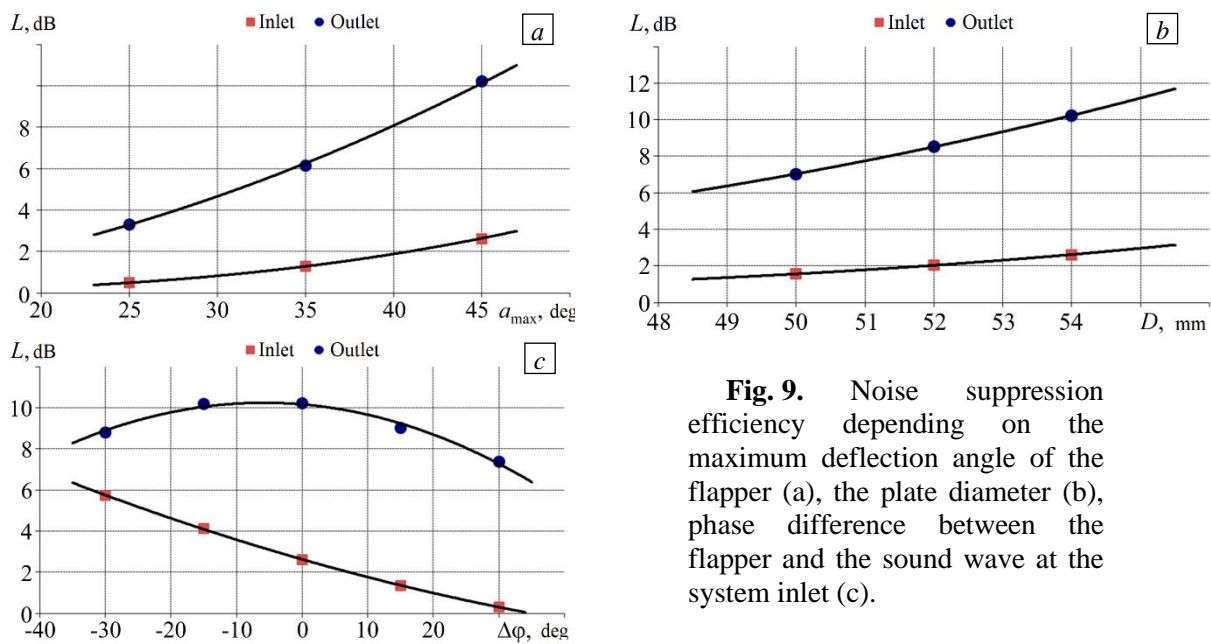
Fig. 9. Noise suppression efficiency depending on the maximum deflection angle of the flapper (a), the plate diameter (b), phase difference between the flapper and the sound wave at the system inlet (c).

5. Conclusion

Numerical modeling of an active noise reduction system in the exhaust pipe of an internal combustion engine has been performed. It is proposed to place an additional controlled sound source in the exhaust pipe, which is opposite in phase to the sound waves coming from the engine. The round plate performed rotational oscillations with controlled frequency and amplitude is considered as the sound source. The influence of the parameters of the incoming sound wave on effectiveness of the active noise suppression system of an internal combustion engine has been studied.

Calculations have shown that the active noise reduction system with considered design solution can reduce noise intensity level by 10 dB. The dependences of the amplitude of fluctuations of static and total pressures at the outlet of the noise suppression system on the amplitude and diameter of the oscillating flapper are obtained. It was found that an increase in the damper radius leads to an increase in the efficiency of the noise reduction system, but at the same time, the aerodynamic resistance that the system exerts to the gas flow significantly increases, which can cause a decrease in engine power. Introduction of an expansion chamber to the system makes it work more efficiently, however, the sound intensity damping rather weakly depends on the volume of the expansion chamber.

References

1. Hirscberg A. Introduction to aeroacoustics and self-sustained oscillations of internal flows. Noise sources in turbulent shear flows: *Fundamentals and applications*, ed. R. Camussi. Springer, 2013. P. 3-72. https://doi.org/10.1007/978-3-7091-1458-2_1
2. Goldstein M.E. *Aeroacoustics*. McGraw-Hill, 1976. 293 p.
3. Morfey C.L. Acoustic energy in non-uniform flow. *J. Sound Vib.*, 1971, vol. 14, pp. 159-170. https://doi.org/10.1016/0022-460X(71)90381-6
4. Ivanov N.I., Nikiforov A.S. *Osnovy vibroakustiki* [Fundamentals of vibroacoustics]. St. Petersburg, Politekhnika, 2000. 482 p.
5. Vasiliev A.V. *Proc. of the 4th International EAA/EEAA symposium "Transport noise and vibration". Tallinn, Estonia, June 8-10, 1998. Pp. 43-46.*
6. Gerges S.N.Y., Jordan R., Thieme F.A., Bento Coelho J.L., Arenas J.P. Muffler modeling by transfer matrix method and experimental verification. *J. Braz. Soc. Mech. Sci. & Eng.*, 2005, vol. 27, pp. 132-140. https://doi.org/10.1590/S1678-58782005000200005
7. Wu C., Chen L., Ni J., Xu J. Modeling and experimental verification of a new muffler based on the theory of quarter-wavelength tube and the Helmholtz muffler. *SpringerPlus*, 2016, vol. 5, 1366. https://doi.org/10.1186/s40064-016-3060-1
8. Lueg P. US Patent No. 2,043,416, 9 June 1936.

9. Vasiliev A.V. *Proc. of the 1997 International Symposium on Active Control of Sound and Vibration. ACTIVE 97, Budapest, Hungary, August 21-23, 1997. Pp. 587-593.*

10. Elliott S. *Proc. of Nordic Acoustical Meeting. NAM'94, Aarhus, Denmark, June 6-8, 1994. Pp. 13-24.*

11. Uchida H., Nakao N., Butsuen T. High Performance active noise control system for engine noise in a car cabin. SAE Paper No. 940608, SAE International, Warrendale, PA, 1994.

12. McDonald A.M., Elliott S.J., Stokers M.A. *Proc. of the Int. Symposium on Active Control of Sound and Vibration. Tokyo, Japan, April 9-11, 1991. Pp. 147-157.*

13. Elliott S.J., Stothers I.M., Nelson P.A., McDonald A.M. Quinn D.C., Saunders T. *Proc. of the Int. Congress on Noise Control Engineering. InterNoise'88, Avignon, France, 30 August-1 September, 1988. Pp. 987-990.*

14. Shih T.-H., Liou W.W., Shabbir A., Yang Z., Zhu J. A new k-ϵ eddy viscosity model for high Reynolds number turbulent flows. *Comput. Fluid.*, 1995, vol. 24, pp. 227-238. https://doi.org/10.1016/0045-7930(94)00032-T

15. Kim S.-E., Choudhury D., Patel B. Computations of complex turbulent flows using the commercial code fluent. *Modeling complex turbulent flows*, ed. M.D. Salas, J.N. Hefner, L. Sakell. Springer, 1999. P. 259-276. https://doi.org/10.1007/978-94-011-4724-8_15

16. Toraño J., Torno S., Menéndez M., Gent M. Auxiliary ventilation in mining roadways driven with roadheaders: Validated CFD modelling of dust behavior. *Tunn. Undergr. Sp. Technol.*, 2011, vol. 26, pp. 201-210. https://doi.org/10.1016/j.tust.2010.07.005